Clipping Noise in OFDM-Based Optical Wireless Communication Systems

Svilen Dimitrov, *Student Member, IEEE,* Sinan Sinanovic, *Member, IEEE,* and Harald Haas, *Member, IEEE*

***Abstract*—In this paper, the impact of clipping noise on optical wireless communication (OWC) systems employing orthogonal frequency division multiplexing (OFDM) is investigated. The two existing optical OFDM (O-OFDM) transmission schemes, asymmetrically clipped optical OFDM (ACO-OFDM) and direct-current-biased optical OFDM (DCO-OFDM), are studied. Time domain signal clipping generally results from direct current (DC) biasing and/or from physical limitations of the transmitter front-end. These include insufficient forward biasing and the maximum power driving limit of the emitter. The clipping noise can be modeled according to the Bussgang theorem and the central limit theorem (CLT) as attenuation of the data-carrying subcarriers at the receiver and addition of zero-mean complex-valued Gaussian noise. Analytical expressions for the attenuation factor and the clipping noise variance are determined in closed-form and employed in the derivation of the electrical signal-to-noise ratio (SNR). The validity of the model is verified through a Monte Carlo bit-error ratio (BER) simulation. Finally, the BER performance of ACO-OFDM with DCO-OFDM is compared for different clipping levels and multi-level quadrature amplitude modulation (M-QAM) schemes.**

***Index Terms*—Wireless communication, optical devices, OFDM, Gaussian processes, non-linear distortion.**

I. Introduction

WITH the advent of incoherent high-power light emitting diodes (LEDs) and highly sensitive photodiodes (PDs), OWC has become a viable candidate for medium range indoor data transmission [1]. As opposed to a radio frequency (RF) system, where the data-carrying signal modulates the electric field radiated by an antenna, in an OWC system the signal modulates the intensity of the optical emitter. Pulsed modulation schemes such as pulse position modulation (PPM), pulse width modulation (PWM) or pulse amplitude modulation (PAM) are often used in OWC systems with intensity modulation and direct detection (IM/DD) [2, 3]. However, the time dispersion of the optical wireless channel in an indoor setup is a major throughput limiting factor for these modulation schemes because of the severe inter-symbol interference (ISI) at high data rates.

A well known modulation technique with an inherent robustness to multi-path dispersion is the OFDM transmission scheme [1, 4]. In O-OFDM, the time domain signal envelope is utilized to modulate the intensity of the LED [4]. For this purpose, the signal needs to be real and non-negative. A real-valued time domain signal is obtained when Hermitian symmetry is imposed on the OFDM subcarriers. One approach to obtain a non-negative signal, known as DCO-OFDM, is the addition of a DC bias [5]. A closely related technique, the discrete multi-tone (DMT) modulation, has been employed for digital subscriber line (DSL) data transmission [6]. Another approach, known as ACO-OFDM, is proposed by Armstrong *et al.* [7–9]. In comparison to DCO-OFDM, ACO-OFDM achieves an increase in the optical power efficiency at the expense of a 50% reduction in spectral efficiency. By enabling the odd subcarriers for data transmission and setting the even ones to zero, the negative part of the time domain signal can be clipped at the transmitter without any information loss. The information can be still successfully decoded from the odd subcarriers at the receiver.

Imperfections of the optical front-ends due to the use of off-the-shelf components result in a non-linear distortion of the transmitted signal such as non-linear transfer effects or signal clipping. An OFDM system employs the inverse fast Fourier transform (IFFT) as a multiplexing technique at the transmitter. Therefore, the non-distorted time domain signal follows a close to Gaussian distribution for large IFFT sizes according to the CLT [10]. A total subcarrier number as small as 64 is sufficient to ensure Gaussianity [11]. As a result, the non-linear distortion can be modeled by means of the Bussgang theorem [12] as an attenuation of the data-carrying signal plus a non-Gaussian uncorrelated clipping noise component [11, 13, 14]. At the receiver, the fast Fourier transform (FFT) is used for demultiplexing. Therefore, the CLT can be applied again, and the clipping noise component can be modeled as a Gaussian process. This methodology is used in [11], where the non-linear transfer effects due to the short dynamic range of high-power amplifiers (HPA) in OFDM-based RF systems are studied. In OWC, the non-linear transfer characteristic of the LED can be compensated by pre-distortion [15]. Symmetric signal clipping due to the large peak-to-average-power ratio (PAPR) in RF OFDM is studied in [16, 17]. Equivalently, symmetric signal clipping in optical OFDM, *e.g.* DMT for DSL transmission, is investigated in [13, 14, 18]. An optimal DC bias of a symmetrically clipped signal can be inferred from [19]. In a previous study [20], bottom level single-sided time domain signal clipping in ACO-OFDM is investigated and the clipping noise statistics are derived in a semi-analytical fashion. However, in OWC the time domain signal is likely to be clipped double-sidedly, *i.e.* to have downside and upside clipping, because of insufficient

Paper approved by W. Shieh, the Editor for Optical Transmission and Switching of the IEEE Communications Society. Manuscript received September 6, 2010; revised March 21, 2011 and July 28, 2011.

This work was presented in part at the *IEEE International Communications Conference ICC 2011*, Kyoto, Japan and at the *IEEE Global Communications Conference GLOBECOM 2011*, Houston, Texas, USA.

The authors are with the University of Edinburgh, Institute for Digital Communications, Joint Research Institute for Signal and Image Processing, Edinburgh EH9 3JL, UK (e-mail: {s.dimitrov, s.sinanovic, h.haas}@ed.ac.uk).

Digital Object Identifier 10.1109/TCOMM.2012.022712.100493

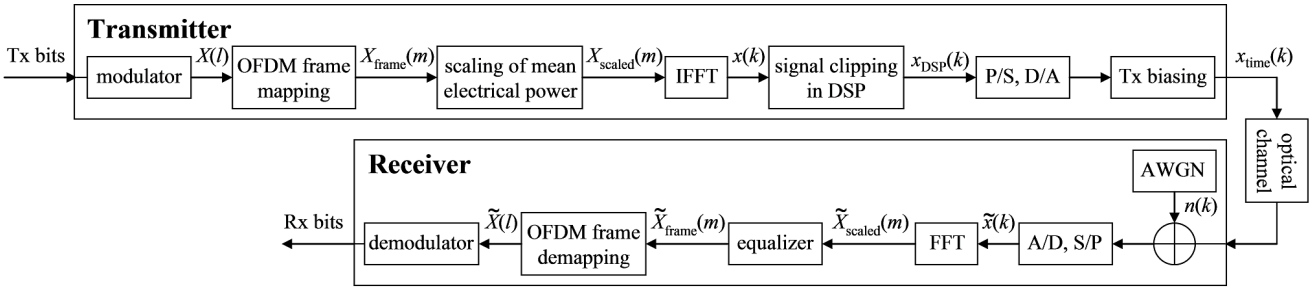

Fig. 1. Block diagram of the OFDM-based OWC system.

forward biasing and the maximum power driving limit of the transmitter front-end. Since, in addition, the eye safety regulations [21] constrain the level of radiated average optical power, the real-valued Gaussian time domain signal in OFDM-based OWC systems is likely to be clipped at independent bottom and top levels.

In this paper, double-sided time domain signal clipping at the transmitter front-end is studied for ACO-OFDM and DCO-OFDM. The attenuation factor and the variance of the complex-valued Gaussian clipping noise at the received data-carrying subcarriers are determined in closed-form and included in the derivation of the electrical SNR. The theoretical BER performance of clipped ACO-OFDM and DCO-OFDM is verified through a Monte Carlo simulation for different clipping levels. Finally, the impact of the clipping distortion on higher order modulation and higher IFFT/FFT sizes is discussed. As a result, the developed framework for signal shaping and biasing in ACO-OFDM and DCO-OFDM can be used to translate the signal scaling and DC biasing for a given dynamic range of the emitter into electrical SNR, and therefore, to BER performance.

The rest of the paper is organized as follows. Section II presents the model of the OFDM-based OWC system. Section III explains the derivation of the clipping noise statistics and the electrical SNR. BER performance results are discussed in Section IV. Finally, Section V concludes the paper.

II. OFDM-BASED OWC SYSTEM MODEL

The system model considered in this study is illustrated in Fig. 1. For simplicity, subscripts indicating the ACO-OFDM and DCO-OFDM signals are omitted in this paper, but they can be clearly inferred from the context. First, the input bit stream at the transmitter is mapped to complex symbols, $X(l)$, according to the chosen modulation scheme, *e.g.* M-QAM. For an IFFT/FFT of size N, N subcarriers form an OFDM frame, $X_{\mathrm{frame}}(m)$, $m = 0, ..., N-1$. The two existing multi-carrier optical wireless transmission schemes, ACO-OFDM and DCO-OFDM, utilize a different frame structure. In ACO-OFDM, $N/4$ symbols in $X(l)$, $l = 0, ..., N/4-1$, are mapped onto half of the odd subcarriers, $X_{\mathrm{frame}}(m)$, $m = 1, 3, 5, ..., N/2-1$, whereas the even subcarriers are set to zero. In DCO-OFDM, $N/2-1$ symbols in $X(l)$, $l = 0, ..., N/2-2$, modulate the first half of $X_{\mathrm{frame}}(m)$ leaving the first subcarrier set to zero, *i.e* $m = 1, ..., N/2-1$. In both systems, Hermitian symmetry of the subcarriers is imposed on the second half of the OFDM frame, $X_{\mathrm{frame}}(m)$, $m = N/2, ..., N-1$, in order to ensure a real-valued time domain signal, $x(k)$, $k = 0, ..., N-1$, at the expense of 50% reduction in spectral efficiency. Here, the utilization factor for the double-sided bandwidth B of the OFDM frame is denoted by G_{B}, where $G_{\mathrm{B}} = 0.5$ in ACO-OFDM and $G_{\mathrm{B}} = (N-2)/N$ in DCO-OFDM. Note that because of the different frame structure of ACO-OFDM and DCO-OFDM $x(k)$ has different statistics which are discussed in the next paragraph. In general, in the OFDM framework there exists the flexibility to employ QAM symbols from different modulation orders, M, across the OFDM frame. Square M-QAM constellations, *e.g.* $\{4\mathrm{-QAM}, 16\mathrm{-QAM}, 64\mathrm{-QAM}, ...\}$, are considered. The $G_{\mathrm{B}}N$ M-QAM symbols on the enabled subcarriers have an average electrical power of $P_{\mathrm{s(elec)}} = P_{\mathrm{b(elec)}} \log_2(M)$, where $P_{\mathrm{b(elec)}}$ is the average electrical power of $G_{\mathrm{B}}N$ bits. Because of the fact that the clipping noise is added equally to each symbol in the OFDM frame, irrespectively of the modulation order [11], and for the sake of simplicity, in this study the same modulation order, M, is chosen for the symbols in the OFDM frame.

Conventionally, in OWC the average optical power of the transmitted signal, $x_{\mathrm{time}}(k)$, is defined in the time domain as $\mathrm{E}\left[x_{\mathrm{time}}(k)\right]$. Here, $\mathrm{E}[\cdot]$ stands for the expectation operator. The average electrical power of the signal, however, is defined in the frequency domain as $\mathrm{E}\left[|X_{\mathrm{frame}}(m)|^2\right]$. According to [8], the mean electrical signal power is proportional to the variance of $x(k)$, $\sigma^2_{x(k)}$. Therefore, in order to fix a certain electrical SNR, $\sigma^2_{x(k)}$ needs to be specified accordingly. For this purpose, the subcarriers at the transmitter require a pre-scaling by a factor, α, to obtain $X_{\mathrm{scaled}}(m)$. Following the Parseval theorem and using an unbiased estimator for the variance of $x(k)$, the factor, α, is expressed as follows:

$$\alpha = \sigma_{x(k)} \sqrt{\frac{N-1}{\sum_{m=0}^{N-1} |X_{\mathrm{frame}}(m)|^2}}. \tag{1}$$

For practical IFFT/FFT sizes, *i.e.* $N > 64$, $\mathrm{E}\left[\alpha^2\right]$ can be simplified to $\mathrm{E}\left[\alpha^2\right] = \sigma^2_{x(k)}/G_{\mathrm{B}}$. Before the scaling clock, the average electrical power of the enabled subcarriers, $X_{\mathrm{frame,info}}(m)$, amounts to $P_{\mathrm{s(elec)}} = P_{\mathrm{b(elec)}} \log_2(M) = 1$. Therefore, a time domain signal, $x(k)$, with a variance of $\sigma^2_{x(k)}$ is obtained when the power of the enabled subcarriers is scaled to $P_{\mathrm{s(elec)}}/G_{\mathrm{B}}$, where $P_{\mathrm{s(elec)}} = \sigma^2_{x(k)}$. As a result, the average bit energy, $E_{\mathrm{b(elec)}}$, can be expressed as follows: $E_{\mathrm{b(elec)}} = \sigma^2_{x(k)} / \left(\log_2(M) G_{\mathrm{B}} B\right)$.

Next, the scaled subcarriers are passed through an IFFT block. Without loss of generality, the unitary transform is employed [9]:

$$x(k) = \frac{1}{\sqrt{N}} \sum_{m=0}^{N-1} X_{\text{scaled}}(m) \exp\left(\frac{j2\pi km}{N}\right). \quad (2)$$

In general, a cyclic prefix (CP) is included in OFDM-based systems to combat ISI and inter-carrier interference (ICI). In addition, the CP transforms the dispersive optical wireless channel into a flat fading channel over the subcarrier bandwidth [9]. However, in OWC the CP is shown to have a negligible impact on the electrical SNR requirement and the spectral efficiency [22]. Therefore, for simplicity, it is omitted in the derivations in this study.

In order to efficiently utilize the dynamic range of the digital-to-analog (D/A) converter, any structure-specific signal clipping needs to be performed in the digital signal processor (DSP). Moreover, in order to facilitate a power efficient D/A conversion, further DC biasing is performed in the analog circuitry. Therefore, the constraints imposed by the emitter front-end need to be pre-set in the DSP signal shaping block which results in signal pre-clipping. In general, the LED is biased by a constant current source which supports the entire range of forward voltages across the LED. The bias current is added to the data-carrying current, yielding the forward current through the LED. Since the radiated optical power is directly proportional to the forward current, the signal and the constraints imposed by the transmitter front-end are described in terms of optical power in the rest of the paper. It is shown in [15] that the non-linear I-V characteristic of the LED can be compensated by pre-distortion. A linear characteristic is obtainable, however, only over a limited range between $i_{\min}$ and $i_{\max}$. Therefore, in this paper, a linear dynamic range of the LED is assumed between a corresponding point of minimum optical power, $P_{\text{Tx,min}}$, and a point of maximum optical power, $P_{\text{Tx,max}}$. The amount of optical power needed to bias the time domain signal is denoted as $P_{\text{Tx,bias}}$.

Because of the time domain signal structure in ACO-OFDM and DCO-OFDM, different combinations of front-end biasing parameters, *i.e.* $\sigma_{x(k)}$ and $P_{\text{Tx,bias}}$, are chosen for a particular linear dynamic range, $P_{\text{Tx,min}}$ to $P_{\text{Tx,max}}$. Therefore, in the two systems the time domain signal, $x(k)$, is pre-clipped at different bottom and top levels, $\varepsilon_{\text{bottom}}$ and ε_{top}. In ACO-OFDM, in the case of insufficient forward biasing, *i.e.* $P_{\text{Tx,bias}} < P_{\text{Tx,min}}$, the signal is pre-clipped at a positive bottom level defined as $\varepsilon_{\text{bottom}} = P_{\text{Tx,min}} - P_{\text{Tx,bias}}$. In the opposite case, *i.e.* $P_{\text{Tx,bias}} \geq P_{\text{Tx,min}}$, $\varepsilon_{\text{bottom}}$ is kept at zero, in order to facilitate the structure-specific asymmetric zero-level signal clipping in ACO-OFDM. Therefore, $\varepsilon_{\text{bottom}} = \max\Big(P_{\text{Tx,min}} - P_{\text{Tx,bias}}, 0\Big)$. In addition, the signal is pre-clipped at a top level, $\varepsilon_{\text{top}} = P_{\text{Tx,max}} - P_{\text{Tx,bias}}$. Since the plausible clipping levels satisfy the inequality $\varepsilon_{\text{bottom}} < \varepsilon_{\text{top}}$, the clipping levels in ACO-OFDM assume only non-negative values. Here, the scenario with the least signal clipping is defined as: $\varepsilon_{\text{bottom}} = 0$ and $\varepsilon_{\text{top}} = +\infty$. In DCO-OFDM, in the case of insufficient forward biasing, *i.e.* $P_{\text{Tx,bias}} < P_{\text{Tx,min}}$, the signal is pre-clipped at a bottom level $\varepsilon_{\text{bottom}} = P_{\text{Tx,min}} - P_{\text{Tx,bias}}$. Moreover, the signal is pre-clipped at a top level, $\varepsilon_{\text{top}} = P_{\text{Tx,max}} - P_{\text{Tx,bias}}$. In DCO-OFDM, the clipping levels can be negative and/or positive as long as the inequality $\varepsilon_{\text{bottom}} < \varepsilon_{\text{top}}$ is satisfied for reasons of plausibility. Here, the scenario with the least signal clipping is defined as: $\varepsilon_{\text{bottom}} = -\infty$ and $\varepsilon_{\text{top}} = +\infty$. As a result of the signal pre-clipping in the DSP, the discrete signal $x_{\text{DSP}}(k)$ is obtained. After parallel-to-serial (P/S) and D/A conversion and addition of the biasing optical power, $P_{\text{Tx,bias}}$, the signal is passed to the optical emitter. In both systems, the DC bias is employed to facilitate the minimum signal clipping. While the unipolar ACO-OFDM signal requires the DC bias only to overcome the minimum required optical power, $P_{\text{Tx,min}}$, the bipolar DCO-OFDM needs a larger DC bias, in order to have its mean placed in the middle of the dynamic range, ensuring minimum bottom and top level clipping [6]. Biasing of both ACO-OFDM and DCO-OFDM time domain signals reveals the trade-off between downside and upside clipping distortion which is discussed in the following Section III. Particular examples for signal biasing are discussed in Section IV. Furthermore, it is important to mention that the addition of the DC bias influences the useful electrical power of the biased time domain signal, $x_{\text{time}}(k) = x_{\text{DSP}}(k) + P_{\text{Tx,bias}}$, to be transmitted. The total electrical power, $\mathrm{E}\left[x_{\text{time}}(k)^2\right]$, is a summation of the useful electrical alternating current (AC) power and the electrical DC power. Therefore, for a fixed total electrical power, the addition of the DC bias reduces the useful electrical AC power of the signal. The attenuation factor, G_{DC}, for the useful electrical AC power is derived at the end of Section IV.

The biased time domain signal, $x_{\text{time}}(k)$, represents the OFDM symbol to be transmitted. After passing through the optical wireless channel, it is received by the optical detector, a combination of a PD and a transimpedance amplifier (TIA). The impulse response of the optical wireless channel can be modeled by a rapidly decaying exponential function with root-mean-square (RMS) delay spreads between 1.3 ns and 13 ns for line-of-sight (LOS) and non-line-of-sight (NLOS) links [2]. In O-OFDM, the ISI from maximum delay spreads of up to 100 ns can be compensated by a CP of 2 samples at a sampling rate of 20 MHz for a negligible reduction of the electrical SNR requirement and the spectral efficiency [22]. Therefore, the channel can be safely considered as flat fading over the entire OFDM frame for bandwidths up to 20 MHz [2, 9], and it can be primarily characterized by the optical path gain coefficient, $g_{\text{h(opt)}}$ [23, 24]. Here, $g_{\text{h(opt)}} = I_{\text{PD}} S_{\text{PD}} \rho_{\text{PD}} G_{\text{TIA}} / (\mathrm{E}\left[x_{\text{time}}(k)\right] \sqrt{r_{\text{load}}})$, where I_{PD} denotes the average irradiance of the PD, S_{PD} is the photosensitive area of the PD, ρ_{PD} is the responsivity of the PD, G_{TIA} is the gain of the transimpedance amplifier (TIA), $\mathrm{E}\left[x_{\text{time}}(k)\right]$ is the average transmitted optical power, and r_{load} is the load resistance over which the received current is measured [24, 25]. Furthermore, it is unlikely that the signal is upside-clipped at the receiver. For instance, the linear range of a Vishay TEMD5110X01 PD reaches up to 0.2 mW of incident optical power at room temperature [26]. For a practical indoor path loss range between 50 dB to 80 dB [23, 24], the transmitter needs to radiate more than 20 W of optical power, in order to drive the PD to saturation. Since such an amount significantly exceeds the limits imposed by the eye safety regulations [21,

24], it is assumed that the upside clipping occurs only at the transmitter. At the detector, the signal is distorted by a zero-mean real-valued bipolar additive white Gaussian noise (AWGN), $n_{\mathrm{AWGN}}(k)$ [8]. It accounts for the shot noise and the thermal noise at the receiver. After optical-to-electrical conversion at the received unequalized constellation, it can be modeled as a zero-mean complex-valued AWGN with a two-sided power spectral density of $N_0/2$ per complex dimension and a variance of $\sigma^2_{\mathrm{AWGN}} = BN_0$ [2, 27].

After serial-to-parallel (S/P) and analogue-to-digital (A/D) conversion the signal is passed through a unitary FFT block back to the frequency domain [9]:

$$\widetilde{X}_{\mathrm{scaled}}(m) = \frac{1}{\sqrt{N}} \sum_{k=0}^{N-1} \widetilde{x}(k) \exp\left(\frac{-j2\pi km}{N}\right). \quad (3)$$

According to [7, 8], in ACO-OFDM the asymmetric clipping at the transmitter results in halving of the amplitude of the odd subcarriers at the receiver. In DCO-OFDM, the subcarrier amplitude is inherently preserved. Therefore, further clipping at the front-ends introduces further attenuation. In general, in the OFDM framework, pilot tones are used for channel estimation and equalization. Thus, by the use of pilot tones within the OFDM frame, the equalization block is able to compensate for the effect of the optical wireless channel and the attenuation due to the signal clipping. Finally, the data-carrying symbols in $\widetilde{X}_{\mathrm{frame}}(m)$ can be extracted due to the known frame structure, and the symbols are demodulated using a maximum likelihood (ML) detector.

III. Assessment of the Clipping Noise Statistics

The clipping of an OFDM time domain signal modifies its mean and consequently its average optical power. Since the non-distorted signal follows a close to Gaussian distribution, the modified mean can be derived based on the statistics of a truncated Gaussian distribution [28]. Thus, the average optical power of the transmitted signal after front-end-induced clipping, $\mathrm{E}[x_{\mathrm{time}}(k)]$, can be expressed as follows:

$$\mathrm{E}[x_{\mathrm{time}}(k)] = \sigma_{x(k)}\Big(\phi(\lambda_{\mathrm{bottom}}) - \phi(\lambda_{\mathrm{top}}) + \lambda_{\mathrm{top}}Q(\lambda_{\mathrm{top}}) - \lambda_{\mathrm{bottom}}Q(\lambda_{\mathrm{bottom}})\Big) + P_{\mathrm{bottom}}\ , \quad (4)$$

where

$$\lambda_{\mathrm{bottom}} = \frac{\varepsilon_{\mathrm{bottom}}}{\sigma_{x(k)}}\ , \quad (5)$$

$$\lambda_{\mathrm{top}} = \frac{\varepsilon_{\mathrm{top}}}{\sigma_{x(k)}}\ , \quad (6)$$

$$\phi(u) = \frac{1}{\sqrt{2\pi}} \exp\left(\frac{-u^2}{2}\right) \quad (7)$$

and

$$Q(u) = \frac{1}{\sqrt{2\pi}} \int_u^{\infty} \exp\left(-\frac{v^2}{2}\right) dv\ . \quad (8)$$

In DCO-OFDM, $P_{\mathrm{bottom}} = P_{\mathrm{Tx,min}}$. In ACO-OFDM, $P_{\mathrm{bottom}} = \max\Big(P_{\mathrm{Tx,min}}, P_{\mathrm{Tx,bias}}\Big)$ because of the default zero-level clipping in the DSP. In general, the eye safety regulations [21] and/or the design requirements constrain the level of radiated average optical power to $P_{\mathrm{Tx,mean}}$. Therefore, $\mathrm{E}[x_{\mathrm{time}}(k)] \leq P_{\mathrm{Tx,mean}}$. Here, $\lambda_{\mathrm{bottom}}$ and λ_{top} are the normalized bottom and top clipping levels relative to a standard normal distribution. In addition, $\phi(\cdot)$ and $Q(\cdot)$ are the respective probability density function (PDF) and complementary cumulative distribution function (CCDF). Plausible clipping levels satisfy the inequality $\lambda_{\mathrm{bottom}} < \lambda_{\mathrm{top}}$. In addition, lower λ_{top} results in larger signal clipping, whereas the opposite holds for $\lambda_{\mathrm{bottom}}$. The scenario with the least signal clipping is defined in ACO-OFDM for $\lambda_{\mathrm{bottom}} = 0$ and $\lambda_{\mathrm{top}} = +\infty$. In DCO-OFDM, the least signal clipping is obtained for $\lambda_{\mathrm{bottom}} = -\infty$ and $\lambda_{\mathrm{top}} = +\infty$. For a given dynamic range of the transmitter, $P_{\mathrm{Tx,min}}$ to $P_{\mathrm{Tx,max}}$, the variables in (4) depend only on $P_{\mathrm{Tx,bias}}$ and $\sigma_{x(k)}$. It can, therefore, be ascertained that the average optical power of the transmitted signal, $\mathrm{E}[x_{\mathrm{time}}(k)]$, is only a function of the front-end biasing parameters, $\sigma_{x(k)}$ and $P_{\mathrm{Tx,bias}}$. In addition, because of the fact that the time domain signal is clipped, the resulting average optical power, $\mathrm{E}[x_{\mathrm{time}}(k)]$, differs from the undistorted optical power of the OFDM symbol, $P_{\mathrm{s(opt)}}$. In general, $P_{\mathrm{s(opt)}}$, is defined for the least signal clipping scenario. In ACO-OFDM, $P_{\mathrm{s(opt)}} = (P_{\mathrm{Tx,bias}} + \sigma_{x(k)}/\sqrt{2\pi})$, whereas in DCO-OFDM, $P_{\mathrm{s(opt)}} = P_{\mathrm{Tx,bias}}$. Combined with (4), these equations can be used to obtain the relation between $\mathrm{E}[x_{\mathrm{time}}(k)]$ and the undistorted optical power of the OFDM symbol, $P_{\mathrm{s(opt)}}$. Therefore, in O-OFDM, for a given set of front-end optical power constraints, $P_{\mathrm{Tx,min}}$, $P_{\mathrm{Tx,mean}}$ and $P_{\mathrm{Tx,max}}$, one can obtain the signal scaling factor, α, for a target signal variance, $\sigma^2_{x(k)}$, and the required DC bias, $P_{\mathrm{Tx,bias}}$, from (1) and (4).

In addition to the modification of the average optical signal power, the front-end-induced signal clipping distorts the data-carrying symbols. An expression for the distorted scaled data-carrying subcarriers at the receiver, $\widetilde{X}_{\mathrm{scaled,info}}(m)$, is derived by the use of the Bussgang theorem and the CLT. First, the Bussgang theorem is used to obtain $\widetilde{x}(k)$ in ACO-OFDM and DCO-OFDM, respectively, as follows:

$$\widetilde{x}(k) = U\big(x(k)\big)g_{\mathrm{h(opt)}}Ax(k) + g_{\mathrm{h(opt)}}n_{\mathrm{c}}(k) + g_{\mathrm{h(opt)}}P_{\mathrm{Tx,bias}} + n_{\mathrm{AWGN}}(k)\ , \quad (9)$$

$$\widetilde{x}(k) = g_{\mathrm{h(opt)}}Ax(k) + g_{\mathrm{h(opt)}}n_{\mathrm{c}}(k) + g_{\mathrm{h(opt)}}P_{\mathrm{Tx,bias}} + n_{\mathrm{AWGN}}(k)\ . \quad (10)$$

Here, $U(\cdot)$ stands for the unit step function which is used to denote the default zero-level clipping of the time domain signal in ACO-OFDM. The theorem states that after the nonlinear clipping distortion the signal is attenuated by a factor, A, and an uncorrelated non-Gaussian clipping noise, $n_{\mathrm{c}}(k)$, is added. In ACO-OFDM, $n_{\mathrm{c}}(k)$ is non-negative and it has a unipolar distribution, whereas in DCO-OFDM the clipping noise component is bipolar. In addition, in ACO-OFDM the amplitude of the received odd subcarriers is reduced by 50% because of the zero-level clipping and the symmetries discussed in [7]. Therefore, in the presence of double-sided clipping in ACO-OFDM, the effective attenuation factor at the received odd subcarriers, K, is related to A as $K = A/2$, where $A = 1$ in the least signal clipping scenario. In DCO-OFDM, $K = A$. Below K is derived for the considered ACO-OFDM and DCO-OFDM systems. Further on, $\widetilde{x}(k)$ is passed through an FFT. Applying the CLT, the distorted scaled

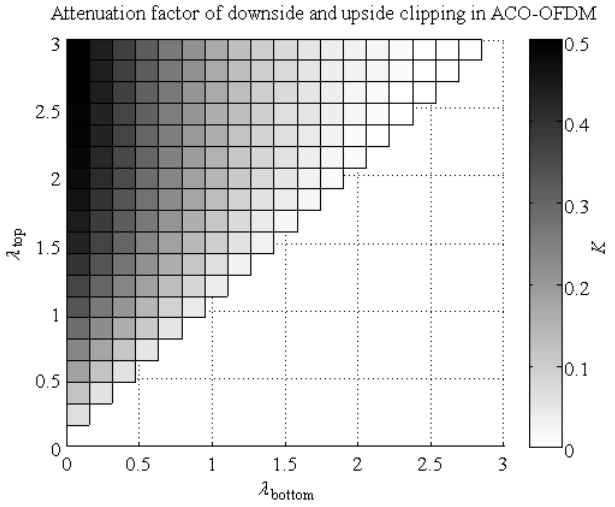

Fig. 2. Attenuation factor of the clipping noise as a function of the normalized clipping levels in ACO-OFDM.

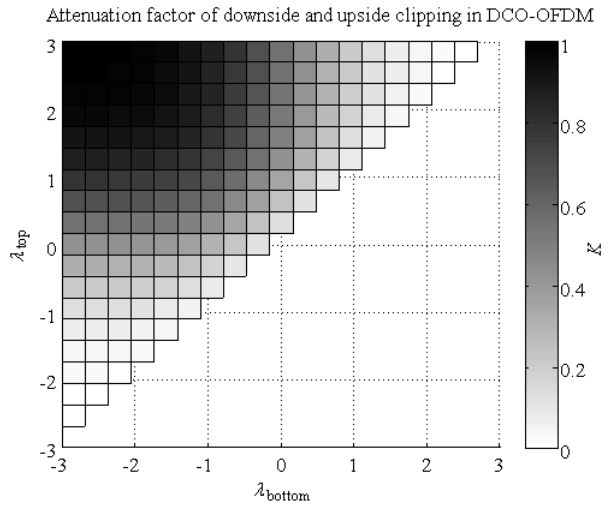

Fig. 3. Attenuation factor of the clipping noise as a function of the normalized clipping levels in DCO-OFDM.

data-carrying subcarriers, $\widetilde{X}_{\text{scaled,info}}(m)$, can be expressed as a function of the transmitted data-carrying subcarriers, $X_{\text{frame,info}}(m)$, in ACO-OFDM and DCO-OFDM as follows:

$$\begin{aligned}\widetilde{X}_{\text{scaled,info}}(m) &= \alpha g_{\text{h(opt)}} K X_{\text{frame,info}}(m) \\ &\quad + g_{\text{h(opt)}}\sigma_{\text{clip}} N_{\mathcal{CN}}(m) + \sigma_{\text{AWGN}} N_{\mathcal{CN}}(m)\ ,\end{aligned} \tag{11}$$

where σ_{clip} is the standard deviation of the complex-valued Gaussian clipping noise at the data-carrying subcarriers. Below we also derive σ_{clip} for the considered ACO-OFDM and DCO-OFDM systems. $N_{\mathcal{CN}}(m)$ is a sample of a complex-valued Gaussian distribution with zero mean and unity variance. Here, in order to recover $X_{\text{frame,info}}(m)$, a zero forcing (ZF) equalizer is employed [3]. Even though ZF is an equalization technique widely used in OFDM-based systems, it results in AWGN amplification when the path gain decreases. Alternatively, minimum mean-squared error (MMSE) equalization can be employed to alleviate this issue [3].

Applying the assumption of Gaussianity of $x(k)$, the attenuation factor, K, is expressed as follows [14]:

$$K = \frac{\text{Cov}\left[x(k), x_{\text{DSP}}(k)\right]}{\sigma^2_{x(k)}} = Q(\lambda_{\text{bottom}}) - Q(\lambda_{\text{top}})\ , \tag{12}$$

where $\text{Cov}[\cdot]$ stands for the covariance operator. Note that in ACO-OFDM and DCO-OFDM, since $x_{\text{time}}(k)$ is real, K is a real-valued function. It essentially represents the likelihood of samples not being clipped. In addition, it proves to be independent of the modulation scheme, M-QAM, and the IFFT/FFT size, N. The attenuation factor as a function of the normalized bottom and top clipping levels is illustrated in Fig. 2 and Fig. 3 for ACO-OFDM and DCO-OFDM, respectively. As suggested in [7, 8], the attenuation factor for ACO-OFDM approaches 0.5 when the least signal clipping is present. Furthermore, the ACO-OFDM symbol suffers larger attenuation for downside clipping as compared to upside clipping. On the contrary, the signal clipping in DCO-OFDM exhibits a symmetric attenuation profile for clipping levels located symmetrically around the average optical power level.

According to (9) and (10) the time domain clipping noise, $n_{\text{c}}(k)$, is an independent component and can be estimated separately. The time domain signal, subject only to double-sided clipping, $x_{\text{DSP}}(k)$, can be written in ACO-OFDM and DCO-OFDM, respectively, as follows:

$$\begin{aligned}x_{\text{DSP}}(k) &= U\big(x(k)\big)x(k) - \Delta_x(k) \\ &= U\big(x(k)\big)2Kx(k) + n_{\text{c}}(k)\ ,\end{aligned} \tag{13}$$

$$x_{\text{DSP}}(k) = x(k) - \Delta_x(k) = Kx(k) + n_{\text{c}}(k)\ . \tag{14}$$

Here, $\Delta_x(k)$ is the clipped signal portion. Therefore, the time domain clipping noise component, $n_{\text{c}}(k)$, can be expressed in ACO-OFDM and DCO-OFDM, respectively, as follows:

$$n_{\text{c}}(k) = U\big(x(k)\big)(1-2K)x(k) - \Delta_x(k)\ , \tag{15}$$

$$n_{\text{c}}(k) = (1-K)x(k) - \Delta_x(k)\ . \tag{16}$$

Because of the unitary FFT at the receiver, $n_{\text{c}}(k)$ is transformed into a zero-mean Gaussian noise component at the data-carrying subcarriers according to the CLT. In order to obtain the clipping noise variance, σ^2_{clip}, the time domain signal in the DSP, $x_{\text{DSP}}(k)$, is required. The later signal is depicted in Fig. 4 and Fig. 5 in ACO-OFDM and DCO-OFDM, respectively. In ACO-OFDM, the symmetries discussed in [7] allow the unfolding of the truncated half Gaussian distribution of $x_{\text{DSP}}(k)$, the mirroring of the clipping levels around the origin and the redistribution of the signal samples. The resulting signal is denoted as $\hat{x}_{\text{DSP}}(k)$, and it is depicted in Fig. 6. It is a symmetric signal with respect to the origin, and it follows a close to Gaussian distribution with zero mean and variance of $P_{\text{s(elec)}}/2$ when the least signal clipping is present. However, $\hat{x}_{\text{DSP}}(k)$ has a bias of $-\sigma_{x(k)}\lambda_{\text{bottom}}/\sqrt{2}$ on the negative samples and a bias of $\sigma_{x(k)}\lambda_{\text{bottom}}/\sqrt{2}$ on the positive ones. Since these biases are to be mounted on the first subcarrier in the ACO-OFDM frame after the FFT, they are irrelevant to the clipping noise variance on the data-carrying subcarriers. Thus, $\hat{x}_{\text{DSP}}(k)$ is debiased to obtain $\hat{x}_{\text{DSP,debiased}}(k)$ as illustrated in Fig. 7. Using the statistics of a truncated Gaussian distribution, σ^2_{clip} can be expressed in ACO-OFDM as follows:

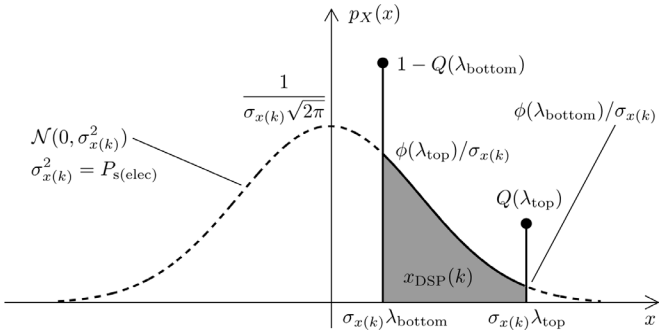

Fig. 4. Time domain signal in DSP, $x_{\text{DSP}}(k)$, in ACO-OFDM.

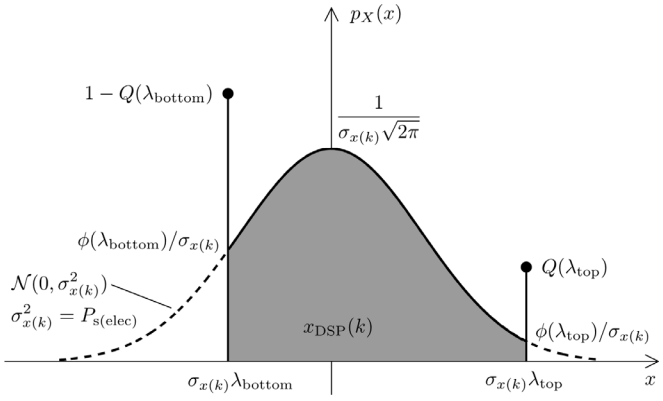

Fig. 5. Time domain signal in DSP, $x_{\text{DSP}}(k)$, in DCO-OFDM.

$$\sigma^2_{\text{clip}} = \frac{P_{\text{s(elec)}}}{2}(1-4K^2) - \Delta\sigma^2 \ , \tag{17}$$

where

$$\Delta\sigma^2 = \frac{P_{\text{s(elec)}}}{2} - \mathrm{E}\left[\hat{x}_{\text{DSP,debiased}}(k)^2\right] \ , \tag{18}$$

$$\begin{aligned}\mathrm{E}\left[\hat{x}_{\text{DSP,debiased}}(k)^2\right] = \frac{P_{\text{s(elec)}}}{2}\Big(&4\phi(\lambda_{\text{top}})\lambda_{\text{bottom}} \\ &-2\phi(\lambda_{\text{top}})\lambda_{\text{top}} - 2\phi(\lambda_{\text{bottom}})\lambda_{\text{bottom}} \\ &+\big(\lambda^2_{\text{bottom}}+1\big)\big(1-2Q(\lambda_{\text{top}})\big) \\ &-\big(\lambda^2_{\text{bottom}}+1\big)\big(1-2Q(\lambda_{\text{bottom}})\big) \\ &+2Q(\lambda_{\text{top}})\big(\lambda_{\text{top}}-\lambda_{\text{bottom}}\big)^2\Big) \ .\end{aligned} \tag{19}$$

In DCO-OFDM, $x_{\text{DSP}}(k)$ follows a close to Gaussian distribution with zero mean and variance of $P_{\text{s(elec)}}$ when the least signal clipping is present. After removing the bias of $\mathrm{E}[x_{\text{DSP}}(k)]$, the debiased time domain signal, $x_{\text{DSP,debiased}}(k)$, is obtained as illustrated in Fig. 8. Similarly, using the statistics of a truncated Gaussian distribution, σ^2_{clip} can be expressed in DCO-OFDM as follows:

$$\sigma^2_{\text{clip}} = P_{\text{s(elec)}}(1-K^2) - \Delta\sigma^2 \ , \tag{20}$$

where

$$\Delta\sigma^2 = P_{\text{s(elec)}} - \mathrm{E}\left[x_{\text{DSP,debiased}}(k)^2\right] \ , \tag{21}$$

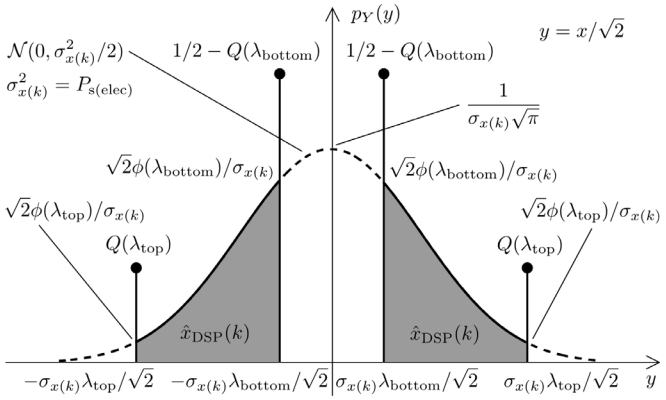

Fig. 6. Unfolded time domain signal in DSP, $\hat{x}_{\text{DSP}}(k)$, in ACO-OFDM.

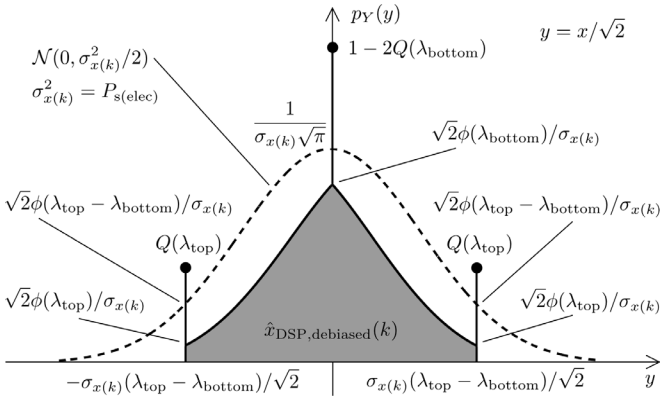

Fig. 7. Debiased and unfolded time domain signal in DSP, $\hat{x}_{\text{DSP,debiased}}(k)$, in ACO-OFDM.

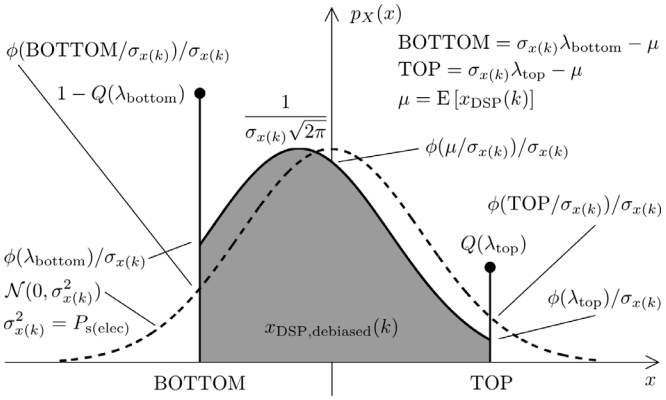

Fig. 8. Debiased time domain signal in DSP, $x_{\text{DSP,debiased}}(k)$, in DCO-OFDM.

$$\mathrm{E}\left[x_{\text{DSP,debiased}}(k)^2\right] = \mathrm{E}\left[x_{\text{DSP}}(k)^2\right] - \mathrm{E}\left[x_{\text{DSP}}(k)\right]^2 \ , \tag{22}$$

$$\begin{aligned}\mathrm{E}\left[x_{\text{DSP}}(k)\right] = \sqrt{P_{\text{s(elec)}}}\Big(&\phi(\lambda_{\text{bottom}}) - \phi(\lambda_{\text{top}}) \\ &+\big(1-Q(\lambda_{\text{bottom}})\big)\lambda_{\text{bottom}} + Q(\lambda_{\text{top}})\lambda_{\text{top}}\Big) \ ,\end{aligned} \tag{23}$$

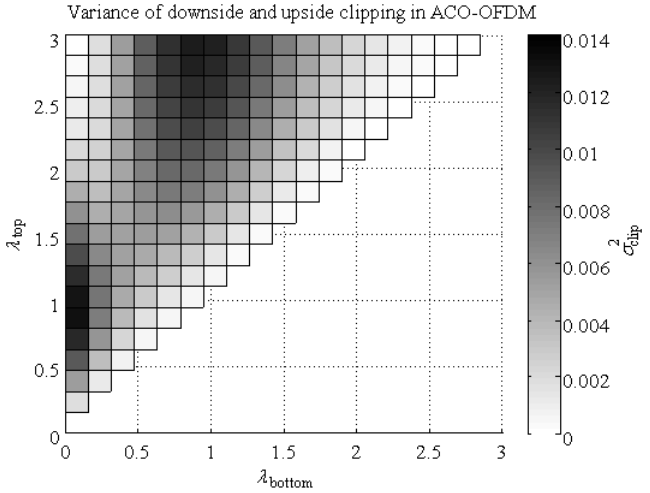

Fig. 9. Variance of the clipping noise as a function of the normalized clipping levels in ACO-OFDM. Here, a scaled symbol power of $P_{\text{s(elec)}}/G_{\text{B}} = 1$ is assumed.

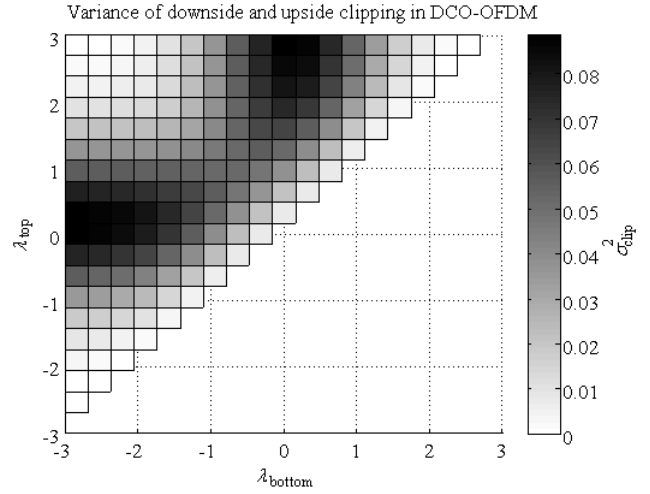

Fig. 10. Variance of the clipping noise as a function of the normalized clipping levels in DCO-OFDM. Here, a scaled symbol power of $P_{\text{s(elec)}}/G_{\text{B}} = 1$ is assumed.

$$\begin{aligned}\mathrm{E}\left[x_{\text{DSP}}(k)^2\right] = P_{\text{s(elec)}}\Big(&Q(\lambda_{\text{bottom}}) - Q(\lambda_{\text{top}}) \\ &+\phi(\lambda_{\text{bottom}})\lambda_{\text{bottom}} - \phi(\lambda_{\text{top}})\lambda_{\text{top}} \\ &+\big(1 - Q(\lambda_{\text{bottom}})\big)\lambda^2_{\text{bottom}} + Q(\lambda_{\text{top}})\lambda^2_{\text{top}}\Big)\,.\end{aligned} \tag{24}$$

Note that similarly to the attenuation factor, K, the clipping noise variance, σ^2_{clip}, is independent of the modulation order, M, and the IFFT/FFT size, N. It only depends on the normalized bottom and top clipping levels. This is illustrated in Fig. 9 and Fig. 10 for ACO-OFDM and DCO-OFDM, respectively. As expected, σ^2_{clip} approaches zero for the least signal clipping scenario. However, since K and σ^2_{clip} are coupled according to (11), as K approaches zero, σ^2_{clip} approaches zero, as well. Here, the large symbol distortion is defined for a small K and a large σ^2_{clip}. Thus, Fig. 2 and Fig. 9 suggest that downside clipping introduces a larger ACO-OFDM symbol distortion than upside clipping. Expectedly, it is shown in Fig. 3 and Fig. 10 that the symbol distortion in DCO-OFDM can be minimized when symmetric normalized clipping levels are chosen. Since K and σ^2_{clip} are independent of M, they remain constant across the modulation orders for a particular choice of normalized bottom and top clipping levels. Nonetheless, the BER performance of the system depends on the granularity of the constellation, where higher order modulation is more vulnerable to Gaussian noise because of the shrinking of the decision regions. Therefore, for a given biasing setup in the dynamic range of the transmitter front-end, the resulting additive noise term of the non-linear clipping distortion more significantly impacts the BER performance of higher order modulation, M-QAM, as shown in Section IV.

Using (11), (12), (17) and (20), an analytical expression for the effective electrical SNR per bit in OFDM-based OWC, $\Gamma_{\text{b(elec)}}$, can be expressed for ZF as a function of the undistorted electrical SNR per bit, $\gamma_{\text{b(elec)}} = E_{\text{b(elec)}}/N_0$, as follows:

$$\Gamma_{\text{b(elec)}} = \frac{K^2 P_{\text{b(elec)}}/G_{\text{B}}}{\sigma^2_{\text{clip}} + \dfrac{G_{\text{B}}\sigma^2_{\text{AWGN}}}{g^2_{\text{h(opt)}} G_{\text{DC}}}} = \frac{K^2}{\dfrac{G_{\text{B}}\sigma^2_{\text{clip}}}{P_{\text{b(elec)}}} + \dfrac{G_{\text{B}}\gamma^{-1}_{\text{b(elec)}}}{g^2_{\text{h(opt)}} G_{\text{DC}}}}\,. \tag{25}$$

The factor G_{DC} denotes the attenuation of the useful electrical signal power of $x_{\text{time}}(k)$ due to the biasing of the transmitter front-end by $P_{\text{Tx,bias}}$ in the least signal clipping scenario. The factor G_{DC} is defined for ACO-OFDM as follows:

$$\begin{aligned}G_{\text{DC}} &= \frac{\mathrm{E}\left[x_{\text{DSP,least}}(k)^2\right]}{\mathrm{E}\left[x_{\text{time,least}}(k)^2\right]} \\ &= \frac{\sqrt{2\pi}\sigma^2_{x(k)}}{\sqrt{2\pi}\sigma^2_{x(k)} + 4\sigma_{x(k)}P_{\text{Tx,bias}} + 2\sqrt{2\pi}P^2_{\text{Tx,bias}}}\,.\end{aligned} \tag{26}$$

In DCO-OFDM, G_{DC} is given by:

$$G_{\text{DC}} = \frac{\sigma^2_{x(k)}}{\sigma^2_{x(k)} + P^2_{\text{Tx,bias}}}\,. \tag{27}$$

In addition, because of the bias added to the ACO-OFDM signal, $P_{\text{Tx,bias}}$, the electrical-to-optical conversion in [8] has to be generalized as follows:

$$\begin{aligned}P_{\text{s(opt)}} &= \sqrt{\frac{\mathrm{E}\left[x_{\text{time,least}}(k)\right]^2}{\mathrm{E}\left[x_{\text{time,least}}(k)^2\right]}}P_{\text{s(elec)}} \\ &= \sqrt{\frac{2\pi P^2_{\text{Tx,bias}} + 2\sigma_{x(k)}P_{\text{Tx,bias}}\sqrt{2\pi} + \sigma^2_{x(k)}}{2\pi P^2_{\text{Tx,bias}} + 2\sigma_{x(k)}P_{\text{Tx,bias}}\sqrt{2\pi} + \pi\sigma^2_{x(k)}}}P_{\text{s(elec)}}\,.\end{aligned} \tag{28}$$

The conversion in DCO-OFDM given in [8] can be generalized as follows:

$$P_{\text{s(opt)}} = \sqrt{\frac{P^2_{\text{Tx,bias}}}{\sigma^2_{x(k)} + P^2_{\text{Tx,bias}}}}P_{\text{s(elec)}}\,. \tag{29}$$

IV. BER Performance of O-OFDM

The performance of the ACO-OFDM and DCO-OFDM systems in the presence of double-sided signal clipping and AWGN is assessed in terms of BER. The exact closed form expression for the BER performance of M-QAM in AWGN has been presented in [29] as a summation of M terms. A

very good approximation can be obtained by using only the first two terms and neglecting the rest. Therefore, an analytical expression for the BER performance of M-QAM O-OFDM can be obtained as follows:

$$\mathrm{BER} = \frac{4(\sqrt{M}-1)}{\sqrt{M}\log_2(M)} Q\left(\sqrt{\frac{3\log_2(M)}{M-1}\Gamma_{\mathrm{b(elec)}}}\right) + \frac{4(\sqrt{M}-2)}{\sqrt{M}\log_2(M)} Q\left(3\sqrt{\frac{3\log_2(M)}{M-1}\Gamma_{\mathrm{b(elec)}}}\right). \tag{30}$$

The BER performance of O-OFDM with double-sided signal clipping is evaluated as a function of the undistorted electrical SNR per bit, $\gamma_{\mathrm{b(elec)}}$, through the effective electrical SNR per bit in O-OFDM, $\Gamma_{\mathrm{b(elec)}}$. The accuracy of the derived expression for $\Gamma_{\mathrm{b(elec)}}$ is verified by means of a Monte Carlo BER simulation. For this purpose, an IFFT/FFT size of 2048 is chosen. Link parameters such as the optical center frequency, the mutual orientation and position of the transmitter and receiver in an indoor setup and their field of view (FOV), the responsivity and the photosensitive area of the detector, and the average radiated optical power of the transmitter determine the optical path gain coefficient, $g_{\mathrm{h(opt)}}$ [24, 25]. Since, however, $g_{\mathrm{h(opt)}}$ is merely a factor in the equalization process as shown in (11) and (25), a change in $g_{\mathrm{h(opt)}}$ results in an equal SNR penalty in ACO-OFDM and DCO-OFDM. Therefore, $g_{\mathrm{h(opt)}} = 1$ is assumed for simplicity. In addition, based on the optical center frequency, the optical emitter can be modulated within a certain modulation bandwidth. Here, the multiplication of the modulation bandwidth and the spectral efficiency of the system yields the system throughout. However, for a fixed SNR, the BER performance is independent of the bandwidth, and consequently of the throughput. Therefore, the ACO-OFDM and DCO-OFDM systems are constrained for unity bandwidth. In general, because of the structure of the OFDM frame, ACO-OFDM achieves half the spectral efficiency of DCO-OFDM for equal modulation orders. Therefore, in addition to 4-QAM ACO-OFDM with a spectral efficiency of 0.5 bits/s/Hz, 16-QAM ACO-OFDM is compared with 4-QAM DCO-OFDM to evaluate the BER performance at a similar spectral efficiency of 1 bit/s/Hz. Furthermore, the systems are constrained for equal average optical power of the transmitted signal. A practical linear dynamic range of a Vishay TSHG8200 LED between $P_{\mathrm{Tx,min}} = 5$ mW and $P_{\mathrm{Tx,max}} = 50$ mW at room temperature is considered the transmitter [30]. No clipping at the receiver is assumed. As benchmarks for a comparison with existing results, ideal cases for signal scaling and biasing are included from [8]. For any given fixed average optical power at the transmitter, $\mathrm{E}[x_{\mathrm{time}}(k)] = P_{\mathrm{Tx,mean}}$, the ACO-OFDM signal is clipped in the ideal case at $\lambda_{\mathrm{bottom}} = 0$ and $\lambda_{\mathrm{top}} = +\infty$. Here, $P_{\mathrm{Tx,bias}} = 0$ and $\sigma_{x(k)} = P_{\mathrm{Tx,mean}}\sqrt{2\pi}$. In DCO-OFDM, a widely used ideal case is defined for $\lambda_{\mathrm{bottom}} = -2$ and $\lambda_{\mathrm{top}} = +\infty$ [8]. Here, $P_{\mathrm{Tx,bias}} = P_{\mathrm{Tx,mean}}$ and $\sigma_{x(k)} = P_{\mathrm{Tx,mean}}/2$. In addition to the ideal case, two clipping scenarios which satisfy the average optical power constraint are considered for the verification of the analytical framework, following the guidelines for signal scaling, clipping and biasing discussed in Section II. Thus, two average optical power constraints are chosen, *i.e.* $\mathrm{E}[x_{\mathrm{time}}(k)] = P_{\mathrm{Tx,mean}} = 10$ mW and $\mathrm{E}[x_{\mathrm{time}}(k)] = P_{\mathrm{Tx,mean}} = 15$ mW. Here, the front-end biasing is defined through the parameters $P_{\mathrm{Tx,bias}}$ and $\sigma_{x(k)}$. They are obtained from (4) as a pair which yields the chosen $P_{\mathrm{Tx,mean}}$ for the given $P_{\mathrm{Tx,min}}$ and $P_{\mathrm{Tx,max}}$. In the first case, $P_{\mathrm{Tx,mean}} = 10$ mW is realized in ACO-OFDM for $P_{\mathrm{Tx,bias}} = 4.2$ mW and $\sigma_{x(k)} = 14.5$ mW, whereas $P_{\mathrm{Tx,bias}} = 9.8$ mW and $\sigma_{x(k)} = 4.9$ mW are required in DCO-OFDM. In the second case, $P_{\mathrm{Tx,mean}} = 15$ mW is obtained in ACO-OFDM for $P_{\mathrm{Tx,bias}} = 2.8$ mW and $\sigma_{x(k)} = 30.6$ mW, while $P_{\mathrm{Tx,bias}} = 14.8$ mW and $\sigma_{x(k)} = 7.4$ mW are considered in DCO-OFDM. The two biasing setups yield the following normalized clipping levels. In ACO-OFDM, $\lambda_{\mathrm{bottom}} = 0.06$ and $\lambda_{\mathrm{top}} = 3.15$ in the first case, whereas $\lambda_{\mathrm{bottom}} = 0.07$ and $\lambda_{\mathrm{top}} = 1.54$ in the second case. In DCO-OFDM, $\lambda_{\mathrm{bottom}} = -0.98$ and $\lambda_{\mathrm{top}} = 8.2$ in the first case, whereas $\lambda_{\mathrm{bottom}} = -1.32$ and $\lambda_{\mathrm{top}} = 4.76$ in the second case. Since ACO-OFDM is more efficient in terms of optical power, it is expected to perform better in the first biasing setup because of the less severe upside clipping. On the contrary, DCO-OFDM is expected to perform better in the second biasing setup, because the normalized clipping levels are closer to a symmetric clipping.

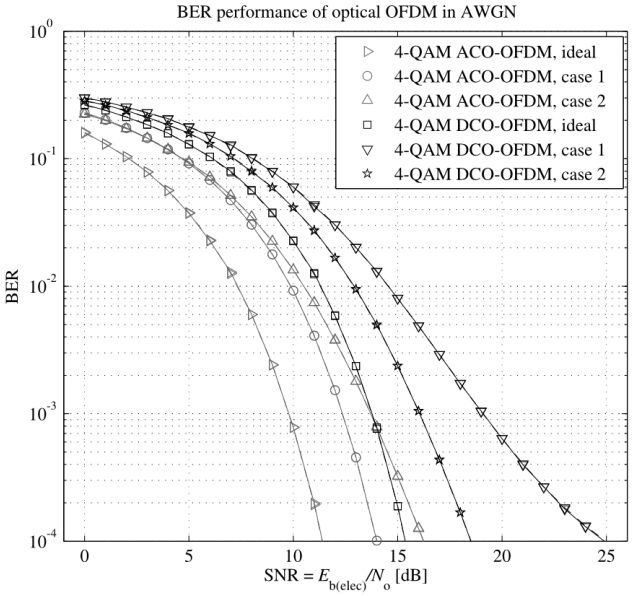

Fig. 11. BER performance of optical OFDM in AWGN, 4-QAM ACO-OFDM *vs.* 4-QAM DCO-OFDM, simulation (solid lines) *vs.* theory (dashed lines).

The BER performance of the studied ACO-OFDM and DCO-OFDM systems is presented in Fig. 11 and Fig. 12. The theoretical and simulation results confirm a very close match. It is shown that the existing simulation results from [8] for an ideal biasing scenario underestimate the BER performance of ACO-OFDM and DCO-OFDM in a biasing setup with a clipping distortion. However, the ideal biasing scenarios are not achievable in practice. In general, for identical QAM modulation orders ACO-OFDM demonstrates a better BER performance as compared to DCO-OFDM at the expense of 50% reduction in spectral efficiency. In Fig. 11, even though 4-QAM ACO-OFDM shows the better BER performance for a

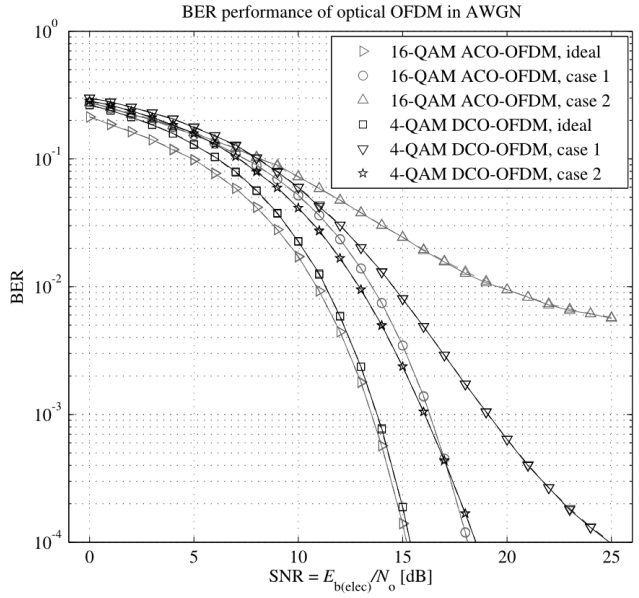

Fig. 12. BER performance of optical OFDM in AWGN, 16-QAM ACO-OFDM *vs.* 4-QAM DCO-OFDM, simulation (solid lines) *vs.* theory (dashed lines).

corresponding clipping scenario, it is outperformed by 4-QAM DCO-OFDM in terms of spectral efficiency over the entire SNR region [20]. However, the results show that the biasing setup plays a significant role when comparing 16-QAM ACO-OFDM and 4-QAM DCO-OFDM. In general, a setup which accommodates a lower average optical power with respect to the given dynamic range is more suitable for ACO-OFDM. However, shifting the average optical power towards the middle of the dynamic range can potentially yield a better BER performance with DCO-OFDM and thereby a higher system throughput. This is because of the resulting front-end-induced signal clipping: in the first case DCO-OFDM is clipped more severely, whereas in the second case ACO-OFDM is the one that suffers a greater signal degradation. This is confirmed by the BER results of 16-QAM ACO-OFDM and 4-QAM DCO-OFDM in Fig. 12. Whereas the first case of 16-QAM ACO-OFDM and the second case of 4-QAM DCO-OFDM perform similarly, the respective counterparts are more severely clipped and show a degraded performance. However, a comparison between 4-QAM and 16-QAM ACO-OFDM suggests that higher order QAM modulation is more vulnerable to signal clipping. This is because, according to (11) the Gaussian clipping noise at the received data-carrying subcarriers is added independently of the QAM modulation order, M. Therefore, it is expected that M-QAM DCO-OFDM delivers a better BER performance and, therefore a higher throughput, as compared to M^2-QAM ACO-OFDM in a biasing setup with a higher average optical power. In addition, since the factors in (11) are independent of N for practical IFFT/FFT sizes, *i.e.* $N > 64$, the BER/throughput performance is independent of the total number of subcarriers.

V. Conclusion

In this paper, double-sided signal clipping in ACO-OFDM and DCO-OFDM OWC systems due to biasing issues and physical limitations of the transmitter front-end is studied. In accord with the Bussgang theorem and the CLT, the statistics of the clipping noise at the received data-carrying subcarriers are derived in closed-form as a function of the normalized bottom and top clipping levels. An expression for the effective electrical SNR per bit in O-OFDM is presented, and it proves to closely match the Monte Carlo BER simulation. The derived SNR shows that, unlike in OFDM-based RF systems, an SNR increase is not achievable simply by increasing the average electrical and/or optical power at the transmitter. In OWC, such a measure leads to a larger clipping distortion, and therefore, to a larger SNR penalty which is exactly quantified in (25). In general, the presented system model includes the power limitations imposed by the transmitter front-end, and it provides means for time domain signal shaping, *i.e.* signal scaling and biasing, to condition the signal within these constraints. It is shown that the BER performance of OFDM-based OWC is more severely degraded with the increase of the modulation order for a particular double-sided signal clipping scenario. In addition, practical IFFT/FFT sizes greater than 64 do not affect the BER performance. Finally, the ACO-OFDM and DCO-OFDM systems are studied for different normalized clipping levels. It is found that ACO-OFDM is more robust to the clipping effects than DCO-OFDM for similar modulation schemes at the expense of a 50% reduction in spectral efficiency. Therefore, ACO-OFDM is more suitable for applications with lower radiated average optical power, whereas DCO-OFDM promises to deliver higher throughput.

Acknowledgement

We gratefully acknowledge EADS UK Ltd. for the support of this research. Professor Haas acknowledges the Scottish Funding Council support of his position within the Edinburgh Research Partnership in Engineering and Mathematics between the University of Edinburgh and Heriot Watt University.

References

[1] Y. Tanaka, T. Komine, S. Haruyama, and M. Nakagawa, "Indoor visible communication utilizing plural white LEDs as lighting," in *Proc. 2001 IEEE International Symp. Personal, Indoor Mobile Radio Commun.*, vol. 2, pp. 81–85.

[2] J. M. Kahn and J. R. Barry, "Wireless infrared communications," *Proc. IEEE*, vol. 85, no. 2, pp. 265–298, Feb. 1997.

[3] J. G. Proakis, *Digital Communications*, 4th edition, ser. McGraw-Hill Series in Electrical and Computer Engineering, S. W. Director, editor. McGraw-Hill Higher Education, Dec. 2000.

[4] H. Elgala, R. Mesleh, H. Haas, and B. Pricope, "OFDM visible light wireless communication based on white LEDs," in *Proc. 2007 IEEE Veh. Technol. Conf. – Spring*.

[5] J. B. Carruthers and J. M. Kahn, "Multiple-subcarrier modulation for nondirected wireless infrared communication," *IEEE J. Sel. Areas Commun.*, vol. 14, no. 3, pp. 538–546, Apr. 1996.

[6] P. Golden, H. Dedieu, and K. Jacobsen, *Fundamentals of DSL Technology*. Auerbach Publications, 2006.

[7] J. Armstrong and A. Lowery, "Power efficient optical OFDM," *Electron. Lett.*, vol. 42, no. 6, pp. 370–372, Mar. 16, 2006.

[8] J. Armstrong and B. J. C. Schmidt, "Comparison of asymmetrically clipped optical OFDM and DC-biased optical OFDM in AWGN," *IEEE Commun. Lett.*, vol. 12, no. 5, pp. 343–345, May 2008.

[9] J. Armstrong, "OFDM for optical communications," *J. Lightwave Technol.*, vol. 27, no. 3, pp. 189–204, Feb. 2009.

[10] J. Rice, *Mathematical Statistics and Data Analysis*, 2nd edition. Duxbury Press, 1995.

[11] D. Dardari, V. Tralli, and A. Vaccari, "A theoretical characterization of nonlinear distortion effects in OFDM systems," *IEEE Trans. Commun.*, vol. 48, no. 10, pp. 1755–1764, Oct. 2000.

[12] J. Bussgang, "Cross correlation function of amplitude-distorted Gaussian signals," Research Laboratory for Electronics, Massachusetts Institute of Technology, Cambridge, MA, Technical Report 216, Mar. 1952.
[13] Q. Pan and R. J. Green, "Bit-error-rate performance of lightwave hybrid AM/OFDM systems with comparison with AM/QAM systems in the presence of clipping impulse noise," *IEEE Photon. Technol. Lett.*, vol. 8, no. 2, pp. 278–280, Feb. 1996.
[14] S. Randel, F. Breyer, S. C. J. Lee, and J. W. Walewski, "Advanced modulation schemes for short-range optical communications," *IEEE J. Sel. Topics Quantum Electron.*, vol. PP, no. 99, pp. 1–10, 2010.
[15] H. Elgala, R. Mesleh, and H. Haas, "Non-linearity effects and predistortion in optical OFDM wireless transmission using LEDs," *Inderscience Intenational J. Ultra Wideband Commun. Syst.*, vol. 1, no. 2, pp. 143–150, 2009.
[16] H. Ochiai and H. Imai, "Performance analysis of deliberately clipped OFDM signals," *IEEE Trans. Commun.*, vol. 50, no. 1, pp. 89–101, Jan. 2002.
[17] A. Bahai, M. Singh, A. Goldsmith, and B. Saltzberg, "A new approach for evaluating clipping distortion in multicarrier systems," *IEEE J. Sel. Areas Commun.*, vol. 20, no. 5, pp. 1037–1046, June 2002.
[18] D. J. G. Mestdagh, P. Spruyt, and B. Biran, "Analysis of clipping effect in DMT-based ADSL systems," in *Proc. 1994 IEEE International Conf. Commun.*, vol. 1, pp. 293–300.
[19] S. C. J. Lee, F. Breyer, S. Randel, H. P. A. van der Boom, and A. M. J. Koonen, "High-speed transmission over multimode fiber using discrete multitone modulation," *J. Optical Netw.*, vol. 7, no. 2, pp. 183–196, Feb. 2008.
[20] S. Dimitrov and H. Haas, "On the clipping noise in an ACO-OFDM optical wireless communication system," in *Proc. 2010 IEEE Global Commun. Conf.*.
[21] BS EN 62471:2008, Photobiological Safety of Lamps and Lamp Systems, BSI British Standards Std., Sep. 2008.
[22] H. Elgala, R. Mesleh, and H. Haas, "Practical considerations for indoor wireless optical system implementation using OFDM," in *Proc. 2009 IEEE International Conf. Telecommun.*
[23] S. Dimitrov, R. Mesleh, H. Haas, M. Cappitelli, M. Olbert, and E. Bassow, "Path loss simulation of an infrared optical wireless system for aircraft," in *Proc. 2009 IEEE Global Commun. Conf.*
[24] ——, "On the SIR of a cellular infrared optical wireless system for an aircraft," *IEEE J. Sel. Areas Commun.*, vol. 27, no. 9, pp. 1623–1638, Dec. 2009.
[25] S. Dimitrov, H. Haas, M. Cappitelli, and M. Olbert, "On the throughput of an OFDM-based cellular optical wireless system for an aircraft cabin," in *Proc. 2011 European Conf. Antennas Propagat.*
[26] Vishay Semiconductors, "Datasheet: TEMD5110X01 Silicon PIN Photodiode," retrieved July 26, 2011 from http://www.vishay.com/docs/84658/temd5110.pdf, May 2009.
[27] D. Tse and P. Viswanath, *Fundamentals of Wireless Communication*. Cambridge University Press, 2005.
[28] N. Johnson, S. Kotz, and N. Balakrishnan, *Continuous Univariate Distributions*, 2nd edition. John Wiley & Sons Ltd., 1994, vol. 1.
[29] J. Li, X. Zhang, Q. Gao, Y. Luo, and D. Gu, "Exact BEP analysis for coherent M-arry PAM and QAM over AWGN and Rayleigh fading channels," in *Proc. 2008 IEEE Veh. Technol. Conf. – Spring*, pp. 390–394.
[30] Vishay Semiconductors, "Datasheet: TSHG8200 High Speed Infrared Emitting Diode, 830 nm, GaAlAs Double Hetero," retrieved July 26, 2011 from http://www.vishay.com/docs/84755/tshg8200.pdf, July 2008.

Svilen Dimitrov (S'09) received the BSc degree in electrical engineering and computer science in 2008, and the MSc degree in communications, systems, and electronics in 2009 from Jacobs University, Bremen, Germany. He wrote his BSc thesis (2007 − 2008) with the department of Pre-Development of Cabin Electronic Systems of Airbus Germany on a simulation model for reproduction of infrared wireless path loss distribution in an aircraft cabin, using a Monte Carlo Ray-tracing algorithm. During his MSc study (2008 − 2009), he extended the work on the characterization of the optical wireless channel with the department of Simulation and Graphical Technologies of EADS Innovation Works Germany. Currently, he is working towards his PhD degree in electrical engineering at the University of Edinburgh, UK. His main research interests are in the area of computer-aided system design, test and optimization with emphasis on wireless communication systems.

Sinan Sinanovic (S'98-M'07) obtained his Ph.D. in electrical and computer engineering from Rice University, Houston, Texas, in 2006. In the same year, he joined Jacobs University Bremen in Germany as a post doctoral fellow. In 2007, he joined the University of Edinburgh in the UK where he currently works as a research fellow in the Institute for Digital Communications (IDCOM). While working with Halliburton Energy Services, he developed acoustic telemetry receiver which was patented. He also worked for Texas Instruments. He is a member of the Tau Beta Pi engineering honor society and a member of Eta Kappa Nu electrical engineering honor society. He won an honourable mention at the International Math Olympiad in 1994.

Professor Harald Haas (S'98-A'00-M'03) received his PhD degree from the University of Edinburgh in 2001. His main research interests are in the areas of wireless system design and analysis as well as digital signal processing, with a particular focus on interference coordination in wireless networks, spatial modulation and optical wireless communication. From 2001 to 2002, Prof. Haas was project manager at Siemens AG (Information and Communication Mobile Networks) for an international research project. He joined International University Bremen, now Jacobs University Bremen, in September 2002 as Associate Professor of Electrical Engineering before returning to the University of Edinburgh in June 2007. He now holds the personal Chair of Mobile Communications in the Institute for Digital Communications (IDCOM). Prof. Haas holds 18 patents in the area of wireless communications. He has published more than 50 journal papers including a Science Article, which is cited more than 400 times, and more than 150 peer-reviewed conference papers. Nine of his papers are invited papers. Prof. Haas has co-authored a book entitled *Next Generation Mobile Access Technologies: Implementing TDD* with Cambridge University Press. This textbook is now being translated into Chinese. His work on optical wireless communication was selected for publication in "100 Produkte der Zukunft (100 Products of the Future)" authored by Nobel Laureate T. W. Hänsch. He was an invited speaker at the TED Global conference 2011. Since 2007 Haas has been a Regular High Level Visiting Scientist supported by the Chinese "111 program" at Beijing University of Posts and Telecommunications (BUPT).